

Microscopic chaos and diffusion

C. P. Dettmann and E. G. D. Cohen

Rockefeller University, 1230 York Ave, New York NY 10021, USA

(December 2, 2024)

We investigate the connections between microscopic chaos, defined on a dynamical level and arising from collisions between molecules, and diffusion, characterized by a mean square displacement proportional to the time. We use a number of models involving a single particle moving in two dimensions and colliding with fixed scatterers. We find that a number of microscopically nonchaotic models exhibit diffusion, and that the standard methods of chaotic time series analysis are ill suited to the problem of distinguishing between chaotic and nonchaotic microscopic dynamics. However, we show that periodic orbits play an important role in our models, in that their different properties in chaotic and nonchaotic systems can be used to distinguish such systems at the level of time series analysis, and in systems with absorbing boundaries. Our findings are relevant to experiments aimed at verifying the existence of chaotic microscopic dynamics in diffusive systems.

I. INTRODUCTION

It is generally assumed that diffusion in macroscopic systems is a result of chaos on a microscopic scale, following Einstein's 1905 explanation for Brownian motion, that is, the movement of a colloidal particle due to thermal fluctuations in the surrounding fluid. Both diffusion and microscopic chaos will be defined with some care below; for now we think of diffusion in terms of the mean square displacement of a particle being proportional to the time and of microscopic chaos (usually shortened to just "chaos") in terms of unpredictability as quantified by positive Lyapunov exponents or a positive Kolmogorov-Sinai entropy. Specifically, a positive Lyapunov exponent of a dynamical system means that initially similar states of the system as measured by distance in phase space separate exponentially fast; the closely related property of positive Kolmogorov-Sinai entropy means that a finite amount of information per unit time is needed to construct the future phase space trajectory of the system, knowing the infinite past trajectory to an arbitrary (but finite) resolution.

A recent experiment of Gaspard et al [1], described below, purports to show that the diffusion of a Brownian particle is due to microscopic chaos. While we believe that Brownian motion (including both the Brownian particle and the solvent) is most likely chaotic, our simulations using nonchaotic models, in a brief Comment [2] and in greater detail here lead to the same results as found in the experiment, so that no experimental proof of microscopic chaos has been given in [1]. Here we explore the question of what kind of experimental measurements or data analysis might be required to identify microscopic chaotic dynamics, and the connection between microscopic chaos and diffusion.

We consider generalizations of models of diffusion due to Lorentz and Ehrenfest (Figs. 1-3), where a single point particle undergoes elastic collisions with a fixed arrangement of circular or square scatterers in two dimensions, respectively. Collisions with the circular scatterers of the (chaotic) Lorentz gas lead to exponential separation of nearby trajectories, that is, a positive Lyapunov exponent, while collisions with the square scatterers of the (nonchaotic) Ehrenfest model lead to at most linear separation of nearby trajectories, and the Lyapunov exponents are all zero. Actually, we consider models with three types of scatterers, all of which are non-overlapping: circles as in the Lorentz gas, squares oriented such that their diagonals are parallel to the coordinate axes and with only four particle velocity directions as in the Ehrenfest wind-tree model, and squares of arbitrary orientations with arbitrary particle velocity directions as a generalization of the Ehrenfest model.

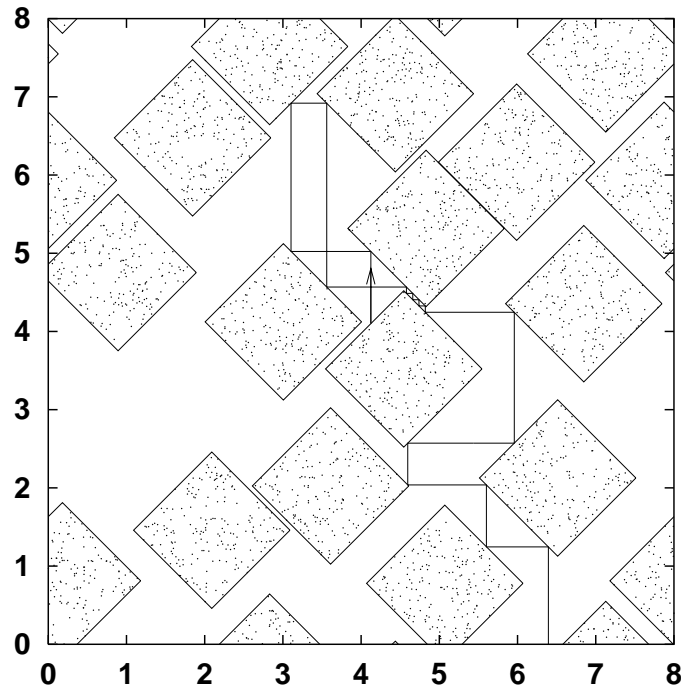


FIG. 1. The fixed orientation wind-tree model. There are periodic boundary conditions, so in the notation of section II C this is FP8.

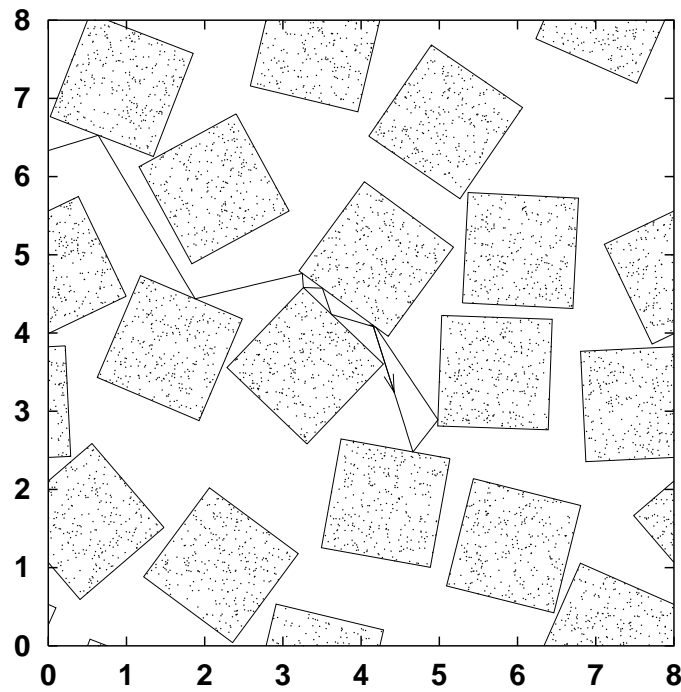


FIG. 2. The randomly oriented wind-tree model, with notation RP8.

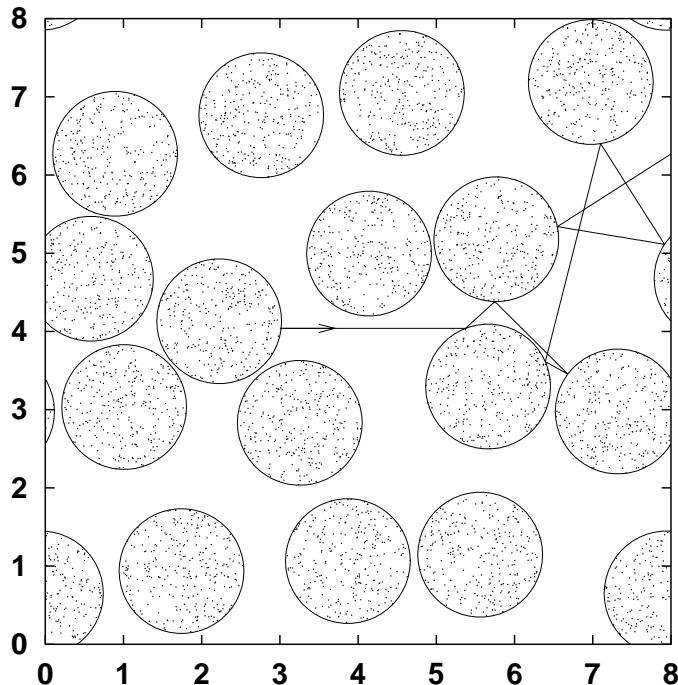


FIG. 3. The Lorentz gas, with notation LP8.

For each of these three models, we consider the following three cases: an infinite number of randomly placed fixed scatterers as in the original models of Lorentz and Ehrenfest, a small number of fixed scatterers in an elementary cell subject to periodic boundary conditions, and an arrangement of a finite number of fixed scatterers enclosed by absorbing boundaries. Note that a model with periodic boundary conditions can be viewed as an infinite periodic system. For the purposes of studying properties such as the mean free time, it is better to view the model as a finite system with periodic boundaries, but to compute the diffusion coefficient in terms of the growth of the mean square displacement with time, it is necessary to view the model as an infinite periodic system.

A link between chaos and diffusion involves a fundamental question of statistical mechanics, since one has to make a connection between the microscopic and macroscopic behavior of large systems. The models we consider here are very special from a physical point of view, but very attractive from a mathematical point of view, because there is only one moving particle, rather than a large number as in, for example, Brownian motion. These can be considered bona fide statistical mechanical models if the large number of scatterers are included, as long as their lack of motion is irrelevant to the questions we ask. We believe that our models incorporate the essential features needed for a discussion of microscopic chaos and diffusion.

We now describe the experiment and analysis of Gaspard et al. in more detail. The position of a Brownian particle in a fluid was measured at regular intervals of $1/60$ s. The experimental time series data was then interpreted using standard techniques of chaotic time series analysis, suggesting a positive lower bound on the Kolmogorov-Sinai entropy, hence microscopic chaos. The method they used, due to Cohen and Procaccia [3] was adapted from an approach pioneered by Grassberger and Procaccia [4]. In this method one analyzes the distribution of recurrences, *i.e.* instances where the system approximately retraces part of its previous trajectory in phase space for a certain length of time, leading to a determination of the Kolmogorov-Sinai entropy. There is detailed mathematical justification for the method (under assumptions such as the length of the data set being sufficient to approximate infinite time limits, see Sec. IV), but the idea is very simple: recurrences give useful information about the predictability of the system. If long recurrences occur very often, it is easy to predict the future of the system from previous instances similar to the recent part of the trajectory, so the system has a small or zero Kolmogorov-Sinai entropy, whereas a rapid decay of the frequency with length of the recurrences indicates a high degree of microscopic chaos. Thus, the Cohen-Procaccia method used by Gaspard can be used to calculate the Kolmogorov-Sinai entropy from a time series in principle, but certain mathematical conditions and limits apply, sometimes restricting

its applicability in practice. Gaspard et al. concluded from their analysis that the Kolmogorov-Sinai entropy of the system containing the Brownian particle was positive, and hence that the microscopic dynamics was chaotic.

Subsequently, we showed [2] that the same approach applied to an “identical” time series generated by a numerical simulation of the nonchaotic (infinite, fixed orientation) Ehrenfest model yielded virtually identical results. This is surprising, since the collisions with the flat sides of square scatterers do not lead to positive Lyapunov exponents, as described above. In Ref. [2] we attributed the discrepancy to the physical issue of time scales — the time interval between measurements (1/60 s) was vastly greater than the typical collision times of the Brownian particle with the solvent particles in the fluid (approximately 10^{-12} s). While this is certainly an experimental problem, it leaves open the question of whether in principle a similar analysis with a much higher resolution could ever prove from experimental data that the microscopic dynamics is chaotic or not.

One aim of the current work is to shed light on this, and related questions. We perform the same Cohen-Proccaccia analysis on all the models mentioned above, finding that the same results are obtained even for a model with a periodic array of squares. This rules out the possibility that the apparently positive value of the Kolmogorov-Sinai entropy is due to a loss of information associated with the randomness of the many scatterers. We discuss the relevant time scales in our models, finding a single microscopic time scale, and we can then qualitatively explain the results of the Cohen-Proccaccia algorithm when the time step is shorter or longer than this time. We conclude that due to the rarity of recurrences in a diffusive system, the determination of chaoticity in such a system requires vastly longer time series than are practical for experimental or computational work, even when the measurements are taken at microscopic time and distance scales.

At that point we return to the question of how microscopic dynamics manifests itself in a time series, as well as in the macroscopic behavior. We develop a new method which we call “almost periodic recurrences” that selects a particular class of recurrences different from those used in the Cohen-Proccaccia method. Our approach is designed to determine only whether a time series is derived from chaotic dynamics or not, but does not determine the value of the Kolmogorov-Sinai entropy quantitatively. We find that, in contrast to the Cohen-Proccaccia method, this method can distinguish between the chaotic Lorentz model and the nonchaotic Ehrenfest model and thus reveals at least one way in which microscopic chaos is manifest, although on macroscopic scales both models exhibit diffusion. The basic idea of our method is simple: almost periodic recurrences are related to periodic orbits which have very different properties in chaotic and nonchaotic systems, so a search for periodic orbits using recurrences may distinguish between the two classes of systems. The positive Lyapunov exponents of chaotic systems (for example the Lorentz gas) ensure that periodic orbits are exponentially unstable, so many repetitions close to a periodic orbit are unlikely. In contrast, the periodic orbits of nonchaotic systems (for example our wind-tree models) can be power law unstable, allowing many repetitions.

The markedly different properties of periodic orbits in the Lorentz and Ehrenfest models leads to the following important observations about diffusion in finite geometries. Solutions of the diffusion equation with absorbing boundaries exhibit exponential decay, corresponding to the probability of a particle remaining in the system for a given time. The randomly oriented wind-tree model has periodic orbits with power law escape, so that the escape from the whole system cannot be exponential at long times. The fixed orientation wind-tree model has no periodic orbits at all, so the particle cannot remain in the system longer than a fixed maximum time. Both of these are examples of situations in which the infinite model satisfies the diffusion equation by having a Gaussian distribution with the mean square displacement proportional to the time, but the corresponding finite model does not satisfy the diffusion equation.

The outline of this paper is as follows: first we introduce our models (Sec. II), and discuss in detail their relevant time scales and chaotic and diffusive properties (Sec. III). Then we discuss the Cohen-Proccaccia method and its inability to distinguish chaotic from nonchaotic dynamics in our case (Sec. IV). Finally we introduce our alternative “almost periodic recurrence” method and discuss the properties of the periodic orbits (Sec. V), and their consequences for finite systems (Sec. VI). We conclude with a discussion of our results and some open questions (Sec. VII).

II. THE MODELS

A. Definitions

The Ehrenfest wind-tree model describes a point “wind” particle moving in straight lines in the plane punctuated by elastic collisions with fixed square scatterers, the “trees”. In the original model (Fig. 1), the trees are oriented with their diagonals along the x and y axes, and the wind particle moves with a fixed velocity in only four possible directions, along these axes. The trees are located at random positions, with a given number density, and not overlapping. There is an overlapping version we will not consider; it exhibits anomalous (sub)-diffusion and non-Gaussian distributions [5].

Secondly, we consider the case of randomly oriented scatterers (Fig. 2), which allows all possible wind particle directions. In both the fixed and randomly oriented cases all Lyapunov exponents are zero, because a collision from a flat scatterer causes only a linear separation of nearby trajectories; it does not cause the exponential separation associated with convex curved scatterers.

Thirdly, we consider the (two dimensional) Lorentz gas (Fig. 3), that is, a model where the scatterers are circular, and we choose the area and number density of the scatterers to correspond to the wind-tree models. This model is known to have normal diffusive properties [6,7] and is used here as a comparison to examine the effects of positive versus zero Lyapunov exponents.

B. Numerical details

For the numerical simulations, we take the velocity of the wind particle to be 1. For the wind-tree models we take the side length l equal to $\sqrt{2}$. This is done for computational convenience; space is divided into unit squares (of side length 1) aligned with the coordinate axes, so that at most one scatterer can be contained in each unit square. For the Lorentz gas the circular scatterers have a radius $R = \sqrt{2/\pi}$ to give them the same area $l^2 = 2$ as the squares. In all cases the total area considered has a number of unit squares, L , up to 3500 in both x and y directions, and periodic boundary conditions are used. To simulate an infinite system, a large value of L (up to 3500) is used; for the maximum time of 10^6 time units the particle never travels far enough to sample the periodic boundary conditions. To simulate a periodic system, a small size such as $L = 4$ is used; we always consider the case of finite horizon, so that the time between collisions is bounded. To simulate a system with absorbing boundaries, an intermediate size such as $L = 20$ is used; the absorbing boundaries are one distance unit inside the edge of the system to avoid the possibility of the particle colliding with a scatterer as well as with its periodic image.

We use a number of scatterers N equal to $L^2/4$. This means that the number density $n = N/L^2$ is $1/4$ in all cases and the proportion of the total area covered by the scatterers is $\rho = N(l/L)^2 = 1/2$. Thus we have an intermediate density of scatterers, which is most convenient from the point of view of the simulations and also the time scales. For a significantly lower density, an infinite horizon is much more likely in all but the largest systems. For a significantly higher density (limited by a maximum of $\rho = 1$) the Metropolis algorithm (see below) used to position the scatterers is very much slower. Also, both for low and high density systems, there is an additional time scale (see section III A), which complicates the analysis.

We now describe the method used to position the fixed scatterers. Each configuration of random positions and orientations is obtained from a version of the Metropolis algorithm, used in [8]. The square scatterers of the wind-tree models are placed initially at points belonging to a square lattice defined such that they do not overlap, that is, with their centers at integer coordinates (m, n) such that $m + n$ is even, and their orientation as in Fig. 1. Not every lattice site is then occupied, depending on the number density.¹ Each scatterer is shifted and rotated a small random amount in turn, typically a few tenths of a distance unit and of order ten degrees respectively. If the shift causes an overlap, the move is rejected and the previous configuration is used. The procedure is repeated with different shifts and rotations. A large fixed number of shifts are attempted, sufficient for reasonable measures of the correlation between scatterers to have long converged to their final values.

¹We use a random initial placement of the scatterers on the lattice to accelerate the convergence of the shifting algorithm, described next. The random placement leads to large scale fluctuations in density. These fluctuations would occur anyway as a result of the small shifts, but only after a very large number of iterations.

If the circles of the Lorentz gas are placed on the same lattice as the squares they overlap slightly; at the chosen density of $\rho = 1/2$ there is enough freedom to allow them to find non-overlapping locations, so that the final configuration is non-overlapping, as we could check. At higher densities circles may not find non-overlapping locations, and a close packed hexagonal lattice should then be used instead.

C. Notation

We now define the notation we will use to distinguish between the various models. There are a very large number of possible parameters that could appear in general, referring to the shape of the scatterers (squares, circles, etc.), different densities and different shaped boundary conditions to name a few, but for conciseness we limit the notation to include only those models we use here, in particular keeping the areal density always at $\rho = 1/2$. Using square brackets [,] to denote different cases, our notation is [F,R,L][∞ ,[P,A]L]. The first symbol [F,R,L] denotes the type and orientation of the scatterers, F for fixed oriented squares, R for randomly oriented squares and L for circles (the Lorentz gas). The next symbol [∞ ,P,A] gives information about the boundary conditions, either ∞ , that is, no boundaries, or P for periodic boundary conditions or A for absorbing boundaries. The symbols P and A are followed by the size of the system, L , which is an even integer. Thus the original Ehrenfest model is denoted $F\infty$, while a periodic Lorentz gas with $L = 8$ (containing $N = L^2/4 = 16$ scatterers at the density used in our simulations) is denoted LP8 (see Fig. 3). The latter model is generated by random shifts of the scatterers as above, ensuring that periodic images of the scatterers do not overlap. When no confusion can arise, we will sometimes refer to classes of models with a simplified notation, for example we denote all randomly oriented wind-tree models as R, and all Lorentz models with absorbing boundaries as LA.

III. FUNDAMENTAL PROPERTIES

A. Time scales

This section collects a number of fundamental properties and results that form a basis for sections IV, V and VI. First we consider the important issue of *time scales*, which puts the time series analysis methods of sections IV and V into a physical context. Then we consider *chaotic properties*, giving known results and conjectures for our models; all of the following sections use this. After this we study *diffusive properties*, obtaining some new results. These are of direct importance to Sec. VI; the time series analysis methods are applied only to our diffusive models,² but the diffusion is somewhat incidental as the methods can be applied to arbitrary time series. At the end of this section we relate the chaotic and diffusive properties of our models.

One of our difficulties of the Gaspard et al experiment [1] is that the interval between their measurements (1/60 s) is so much greater than the relevant time scale (10^{-12} s) of the dynamics, that is the time interval determined by collisions between the Brownian particle and the other particles in the fluid. It is thus important to clarify the issue of what time scales are relevant in our models, so that the simulation results can be put in context. There are three relevant time scales here, the time taken for the particle to traverse the length of a scatterer (defined to be of order one time unit; see Sec. IIB), the mean free time between collisions $\bar{\tau}$, and the time at which the particle begins to notice the finite size L of the system (when it is not infinite). It turns out (see Sec. IIIC) that all the random and periodic models except FP have a well defined diffusion coefficient D , so in these cases the time taken to reach the boundary is of order L^2/D .

The mean free time can be calculated exactly (see the Appendix) and is given by $\bar{\tau}_F = 1$, $\bar{\tau}_R = \pi/(2\sqrt{2}) \approx 1.111$ and $\bar{\tau}_L = \sqrt{\pi/2} \approx 1.253$ for the F, R, and L models respectively, independent of the size of the system (ignoring the case of absorbing boundaries). We have checked these values numerically, and the results agree within their uncertainties of about 0.002. It is clear that all the time scales in these models are of order one time unit, except those defined by the boundary. This

²We include here one model exhibiting superdiffusion, see Sec. IIIC.

means that a time step of one time unit should be sufficient to observe effects due to the microscopic chaos in the time series analysis methods of sections IV and V.

B. Microscopic chaos

We began with the notion of microscopic chaos as the presence of a positive Lyapunov exponent arising from collisions with strictly convex scatterers, or as a positive Kolmogorov-Sinai entropy quantifying the lack of predictability of a chaotic system. We now want to make these ideas more precise and clarify what is known and what is conjectured about our models.

From a mathematical point of view, there are a large number of “chaotic properties” that a system may exhibit [9]. Those of interest to us are

1. Ergodicity. We need ergodicity for the time series analysis methods of Secs. IV and V; that is, a single long trajectory is supposed to sample the dynamics of the whole phase space. We either know or conjecture that ergodicity holds in all of our models (see below).
2. Decay of correlations. We note that Eqs. (6,8) below give the diffusion and Burnett coefficients as integrals over velocity autocorrelation functions. For these coefficients to be defined the appropriate correlations must decay sufficiently quickly.³ Numerical evidence for the existence or nonexistence of these coefficients for our models is given in Sec. III C.
3. A positive Lyapunov exponent, corresponding to exponential separation of initially close trajectories, follows from the shape of the scatterers. The Lorentz gas has a positive Lyapunov exponent due to its convex scatterers, while the wind-tree models have all zero Lyapunov exponents due to their (piecewise) flat scatterers.⁴
4. A positive Kolmogorov-Sinai entropy, which the Cohen-Procaccia method (see Sec. IV) is designed to compute. We either know or conjecture that the KS entropy is equal to the sum of the positive Lyapunov exponents in our models (Pesin’s theorem, see below). Actually there is at most one positive Lyapunov exponent in these systems.
5. Periodic orbit properties that depend on chaoticity are described in Sec. V and used in Secs. V and VI.

We now briefly discuss what is known about our models regarding these chaotic properties. The periodic Lorentz gas has exponential decay of (all two time) correlations [10], which implies ergodicity and the convergence of the integral in (6) below. For (8) see Ref. [11]. The periodic wind-tree models are generically⁵ ergodic [12]. Pesin’s theorem holds for all of these [F,R,L]P models, see Refs. [9,13] for the Lorentz gas and Ref. [12] for the wind-tree models.

The infinite models are much more difficult to treat rigorously because the phase space is not compact. In order to make reasonable conjectures about the above properties, we use the solution of the diffusion equation (2) below, which is verified numerically in Sec. III C for the models [F,R,L] ∞ , to argue that the number of different scatterers hit by the particle in time t is proportional to $t/\log t$, as follows. In two dimensions, the probability density of the particle being at any point decays as $1/t$. This means that in a time t , the particle comes close (say, within a radius ϵ) to the point a number of times proportional to the integral of $1/t$, that is $\log t$. If the point corresponds to the location of a scatterer, we could say that the particle collides with each scatterer a number of times proportional to $\log t$. In this case the total number of different scatterers hit by the particle in time t might be expected to grow proportional to $t/\log t$, which is what we find numerically in Fig. 4.

³Mixing (which implies ergodicity) is equivalent to the statement that all two time correlation functions decay. It is neither necessary nor sufficient for the existence of the diffusion coefficient: it is not necessary because correlations other than velocity correlations need not decay in a diffusive system, and it is not sufficient because the velocity correlation could decay too slowly for the integral to converge.

⁴We are not interested in the exact value of the Lyapunov exponent in the Lorentz gas (although it is easy to calculate numerically) because there is no general relation linking it to, for example, the diffusion coefficient. For example, in our wind-tree models the Lyapunov exponent is zero, but the diffusion coefficient remains positive. The same is true for the KS entropy.

⁵The term generic here denotes a positive measure of scatterer configurations, as opposed to initial positions of the particle.

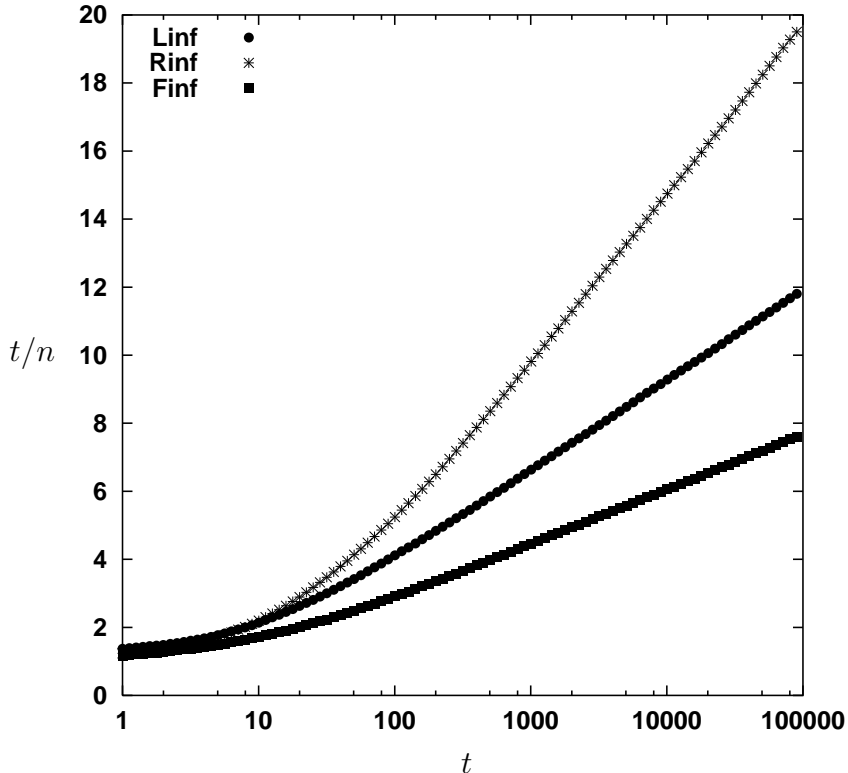


FIG. 4. Numerical evidence for conjectures applying to the infinite models $[F,R,L]\infty$. If n is the average number of *different* scatterers hit by the particle in time t , we expect that n should be roughly proportional to $t/\log t$ for large t . Here we plot t/n as a function of t , which should thus be a straight line on a linear-log scale, as is observed.

These observations have the following consequences for the chaotic properties of the infinite models. Because the particle returns to each scatterer an infinite number of times, we expect that it passes arbitrarily close to every point in phase space, that is, the system is ergodic. The KS entropy gives the amount of information per unit time required to predict the trajectory knowing its infinite past. The unpredictability has two sources, the instability associated with the collisions in the Lorentz gas (that is, the positive Lyapunov exponent), and the random positions of the scatterers with which the particle has not yet collided in all the models. The number of different scatterers hit by the particle grows as $t/\log t$, so the rate decreases to zero as $1/\log t$. We conclude from this argument that the random positions of the scatterers do not contribute to the KS entropy, although results at finite time might suggest otherwise, given that $1/\log t$ decays so slowly. In other words, Pesin's theorem is satisfied for these infinite models also.⁶

Finally, we remark that the qualifier “microscopic” as applied to chaos may be misleading. We use the term “microscopic chaos” to denote the (local) collisions with flat or curved scatterers, however the consequences of many such collisions, positive Lyapunov exponents and so on, are properties of the (global) phase space. The phase space contains detailed (“microscopic”) information about the state of the system, but is not localized in space.

⁶The argument hinges on the solution of the diffusion equation (Eq. (1) below) in two dimensions. In three dimensions, the density decays as $t^{-3/2}$ which is integrable at infinity, so that the particle collides with each scatterer only a finite number of times. This leads to a loss of ergodicity, and a contribution to the KS entropy from the random positions of the scatterers, thus violating Pesin's theorem. There is no contradiction here; the proofs of Pesin's theorem all demand that the phase space be compact.

C. Macroscopic diffusion

Now we discuss diffusive properties. We begin with the diffusion equation, and then relate it to the mean square displacement of a particle. The diffusion equation

$$\frac{\partial P}{\partial t} = D\nabla^2 P \quad (1)$$

for a probability density $P(\mathbf{x}, t)$ with a constant diffusion coefficient D is linear. Thus its general solution is an integral over Green's functions given by the solution for an initial Dirac delta distribution $P(\mathbf{x}, 0) = \delta(\mathbf{x} - \mathbf{x}_0)$, that is,

$$P(\mathbf{x}, t) = (4\pi Dt)^{-d/2} \exp\left[-\frac{(\mathbf{x} - \mathbf{x}_0)^2}{4Dt}\right] \quad (2)$$

is the conditional probability density that a particle initially at the point \mathbf{x}_0 will be at the point \mathbf{x} a time t later; this is therefore a 2-time probability distribution (or density) function. The spatial dimension $d = 2$ in our case.

The diffusion equation is known to hold for the probability density of a particle undergoing deterministic dynamics in a number of systems including the Lorentz gas [7]. In the diffusion equation a macroscopic approximation is used, implying that $P(\mathbf{x}, t)$ is an average over space and time scales large compared to the characteristic microscopic lengths and times of the dynamics. The mean square displacement of the particle in the x -direction after a macroscopic time t is obtained from (2),

$$\langle \Delta x^2 \rangle = \int \Delta x^2 P(\mathbf{x}, t) d\mathbf{x} = 2Dt \quad (3)$$

where $\Delta x = x - x_0$. This is the Einstein relation for diffusion. Note that $x = x(t)$ is now an explicit function of time. Similarly, the fourth and sixth cumulants are

$$\langle \Delta x^4 \rangle_c \equiv \langle \Delta x^4 \rangle - 3\langle \Delta x^2 \rangle^2 = 0 \quad (4)$$

$$\langle \Delta x^6 \rangle_c \equiv \langle \Delta x^6 \rangle - 10\langle \Delta x^4 \rangle \langle \Delta x^2 \rangle + 15\langle \Delta x^2 \rangle^3 = 0 \quad (5)$$

respectively. It is also possible to obtain dimensionless forms of the above expressions dividing them by the appropriate power of $\langle \Delta x^2 \rangle$. In this form the fourth cumulant is usually called the kurtosis, and is a common measure of how close a probability density is to a Gaussian distribution.

Straightforward manipulations applied to the mean square displacement lead to the Green-Kubo expression for the diffusion coefficient (if it exists)

$$D = \int_0^\infty \langle v_t v_0 \rangle dt \quad (6)$$

where v is one (say the x -) component of the velocity and the subscript denotes the time. This shows that the existence of a diffusion coefficient is also related to the rate of decay of the velocity autocorrelation function. The integral diverges if the decay rate of the integrand is t^{-1} or slower, unless the integrand is oscillatory. An oscillatory integrand cannot be ruled out, but is not typical for the Lorentz gas as observed in numerical simulations.

The diffusion equation is the lowest order macroscopic description of the diffusion process. The next approximation, in the direction of microscopic space and time scales, *ie.* when the probability density P varies sufficiently rapidly, the right hand side of Eq. (1) may be augmented by terms such as $B\nabla^4 P$, where B is called the linear super-Burnett coefficient [6]. Like the diffusion coefficient, it obeys an Einstein relation

$$\langle \Delta x^4 \rangle - 3\langle \Delta x^2 \rangle^2 = 24Bt \quad (7)$$

This is consistent with the zero kurtosis found previously (4): to find the kurtosis we divided by $\langle x^2 \rangle^2$ which is proportional to t^2 if the diffusion coefficient exists, while the Burnett coefficient in (7) gives a smaller term (for large t), proportional to t . The Burnett coefficient can also be written in the form of a Green-Kubo relation in terms of integrals over four-time velocity correlation functions,

$$B = \frac{1}{6} \int_0^\infty \int_0^\infty \int_0^\infty (\langle v_0 v_1 v_2 v_3 \rangle - \langle v_0 v_1 \rangle \langle v_2 v_3 \rangle - \langle v_0 v_2 \rangle \langle v_1 v_3 \rangle - \langle v_0 v_3 \rangle \langle v_1 v_2 \rangle) dt_1 dt_2 dt_3 \quad (8)$$

where $v_0 = v(t = 0)$ as above and $v_1 = v(t = t_1)$ etc. A slow decay of the relevant correlation functions leads more easily to a divergence in this case than in Eq. (6) [6]. This means that it is possible to have a well defined diffusion coefficient, but a divergent Burnett coefficient, which occurs if the fourth cumulant increases faster than t but slower than t^2 .

We estimate the cumulants defined in Eqs. (3-5) numerically by choosing a large number (typically 10^5) of random initial conditions for the particle not inside a scatterer, for a single configuration of scatterers. We report only the cumulants in the x -direction, although we have checked that the y distribution is similar. See Figs. 5-7 and Table I.

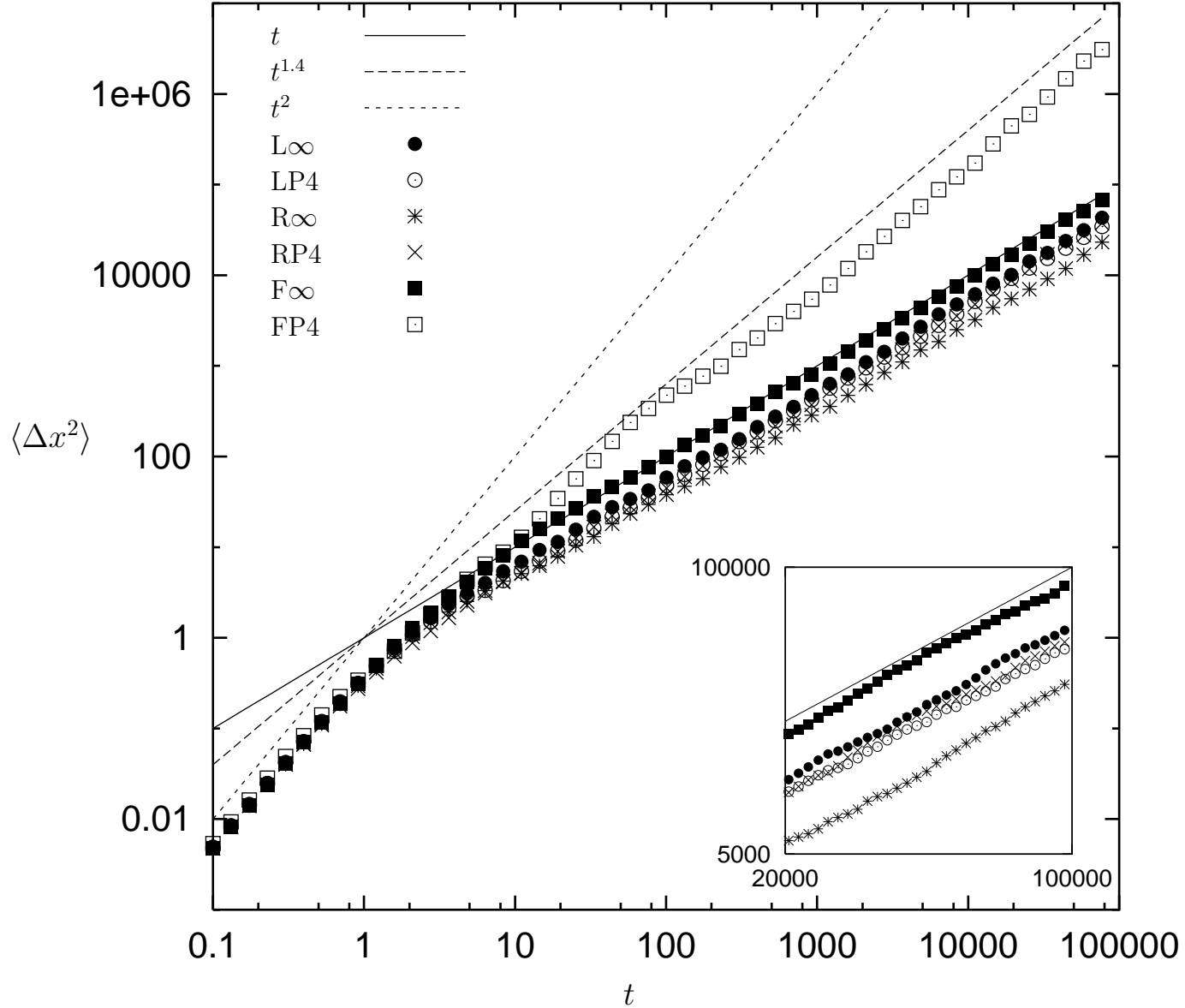


FIG. 5. The mean square displacement (3) for the six models [F,R,L][∞ ,P4]. In each case there is a transition between ballistic behavior $\langle \Delta x^2 \rangle \sim t^2$ to the long time diffusive (or superdiffusive) behavior. The FP4 model is superdiffusive, with an approximate $t^{1.4}$ law; the others exhibit normal diffusion, $\sim t$. The diffusion coefficient is largest for the F ∞ model, followed by L ∞ , RP4, LP4, and R ∞ (inset and Tab. I); see the discussion in the text.

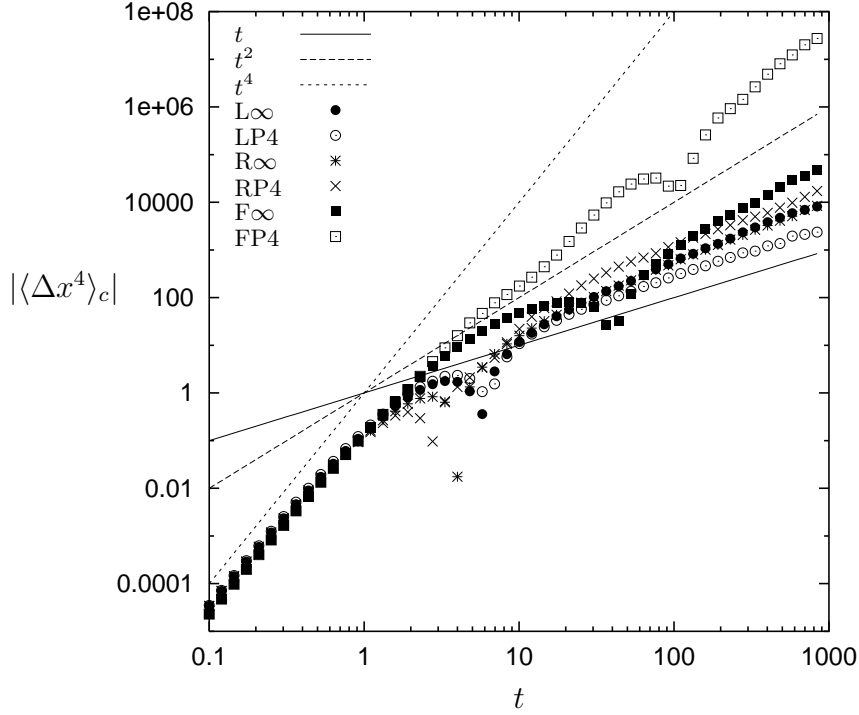


FIG. 6. The fourth cumulant (4) for the six models [F,R,L][∞ ,P4]. We are mostly interested in the long time behavior, which is Gaussian when the fourth cumulant grows more slowly than t^2 , as holds in all models except the superdiffusive FP4 model. The periodic Lorentz gas LP4 has a finite Burnett coefficient, so its fourth cumulant is proportional to t as shown. At short times for all models a ballistic t^4 behavior is followed by an intermediate regime in which all models exhibit a change of sign which appears as a dip due to the logarithmic axes.

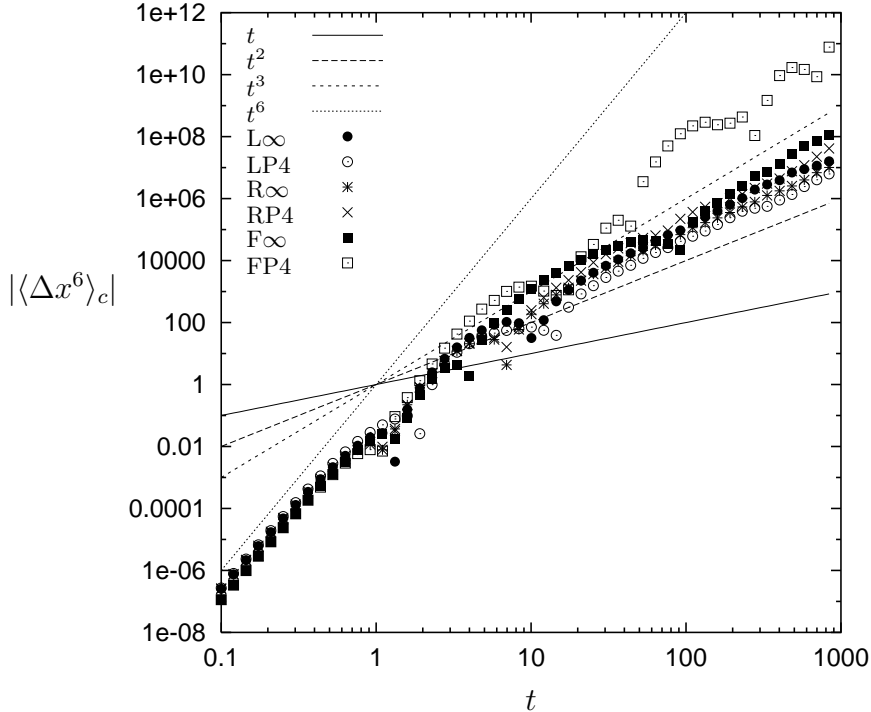


FIG. 7. The sixth cumulant (5) for the six models [F,R,L][∞ ,P4]. The statistics are rather poor in this case, so that delicate cancelations cannot be observed; these curves should be viewed as upper limits on the true values for large times. It is at least plausible that all of the models except FP4 are Gaussian, which is indicated by a growth slower than t^3 . At small times the ballistic regime gives t^6 .

model	F	R	L
∞	$D = 0.44$	$D = 0.14$	$D = 0.27$
P4	-	$D = 0.24$	$D = 0.23, B = 0.12$

TABLE I. Diffusive properties of our models, in terms of the diffusion coefficient D , and the Burnett coefficient B if they exist. The existence of these coefficients is related to the rate of decay of the velocity autocorrelation functions of (6,8). Note that by this criterion, the periodic Lorentz gas LP4 is more “chaotic” than the infinite Lorentz model $L\infty$, while the periodic fixed orientation wind-tree model FP4 is less “chaotic” than the infinite model $F\infty$. Only typical values of the coefficients for the periodic models are given, since they depend on the position of the scatterers.

For five models, [F,R,L] ∞ , [R,L]P4, the mean square displacement is found to be proportional to the time, and the fourth and sixth cumulants increase slower than t^2 and t^3 respectively at large times, indicating that the distribution approaches a Gaussian. The exception to this rule is FP4, for which the mean square displacement grows faster than the time, approximately as $t^{1.4}$ and the kurtosis is also nonzero. This superdiffusive behavior is not particularly stable in the sense that the mean square displacement for this model has larger fluctuations than the other models, and the exponent of approximately 1.4 varies unpredictably between 1 and 2 with the exact positions of the scatterers and the size of the cell (for example for FP6 or FP8).

D. Connections between chaotic and diffusive properties

We now look at how the chaotic and diffusive properties of our models are related in the light of our results, specifically of: (a) normal diffusion without chaos, (b) superdiffusion without chaos, (c) a possible relation between the diffusion coefficient and the periodic orbits, and (d) the Burnett coefficient of the periodic Lorentz gas. In no way does the data presented in Figs. 5-7 distinguish between chaotic and nonchaotic models.

Normal diffusion Our results show that it is possible to have a well defined diffusion coefficient and a Gaussian distribution function without positive Lyapunov exponents, that is, in the F_∞ , R_∞ and RP4 models. The RP4 model is particularly interesting in this regard, since the two most obvious sources of unpredictability: dispersive collisions and collisions with new randomly placed scatterers, are absent. Recall that we argued (in section III B) that these two processes might together determine the KS entropy, that is, the rate of loss of information about the particle's position and velocity. The RP4 model is thus the clearest example of a model in which there is normal diffusion, and zero KS entropy. An example with the same properties, using a periodic rhombus model has been studied in Ref. [14], where a mean square displacement proportional to the time was observed, but the higher moments were not studied.

Superdiffusion The FP4 model, in contrast, has a mean square displacement growing faster than linearly with the time, and a non-Gaussian distribution. This can be related to a slow decay of the velocity autocorrelation function (see above), but a physical explanation of why this occurs in the FP4 model but not in the RP4 model is lacking.

Diffusion and periodic orbits It is perhaps somewhat hazardous to deduce more from this data than the existence of normal diffusion; however we would nevertheless like to point out a possible connection between the value of the diffusion coefficient (given by the vertical displacement of the curves in the inset of Fig. 5) in the infinite models and the properties of periodic orbits discussed in section V. We make no statement about the diffusion coefficient of the periodic models because this coefficient depends on the position of the scatterers. The idea is that the presence of periodic orbits in a model with randomly positioned scatterers might be expected to lower the diffusion coefficient, since the periodic orbits may keep the particle trapped in roughly the same place; this takes time without contributing to the mean square displacement. Thus we observe that the fixed orientation wind-tree model F_∞ has no periodic orbits and has the largest diffusion coefficient; the random Lorentz gas L_∞ has periodic orbits, but they are exponentially unstable, and has the next largest diffusion coefficient; the random orientation wind-tree model R_∞ has periodic orbits with power law instability that can inhibit diffusion for a long time, and the diffusion coefficient is the smallest of the three.

The Burnett coefficient The fourth cumulant grows linearly with time for the LP4 model, indicating a finite Burnett coefficient, as expected, given its exponential decay of correlations [11]. The other models, F_∞ , R_∞ , RP4 and L_∞ have a divergent Burnett coefficient, which is not surprising since their decay of correlations is most likely as a power law. Thus, from the more subtle properties of the two time (displacement) correlation function, we can deduce some properties relating to the rate of decay of higher order correlations, even special four-time (velocity) correlations, but not whether there is a positive Lyapunov exponent, since L_∞ behaves similarly to R_∞ from this point of view. Even in the intermediate region between the ballistic behavior at small times and the (super)-diffusive behavior at large times in Fig. 5, that is, where the distribution functions are measured at microscopic time scales, there is no clear distinction between the chaotic and nonchaotic models.

We have now discussed at some length the connection between chaotic and diffusive properties of our models. While this has yielded valuable insight into how little chaoticity is needed for diffusion to occur, it has not provided us with an understanding of how chaotic and nonchaotic diffusion differ, let alone a method to distinguish chaotic and nonchaotic diffusive systems experimentally. The reason, given in Ref. [15] is that two time correlations (for example our cumulants) are insufficient to characterize chaos; multi-time correlations (or their underlying probability distributions) are required. The remaining sections of this paper all use multi-time distributions of one form or another to investigate our models. We begin with a more detailed study of the Grassberger-Procaccia method than in Ref. [2], where we found it to incorrectly classify the F_∞ model as chaotic.

IV. THE GRASSBERGER-PROCACCIA METHOD

Grassberger and Procaccia [4] gave the earliest practical methods for computing chaotic properties such as entropies and dimensions from experimental or computer generated time series. These are still the most popular methods in use, sometimes with minor variations. In Ref. [1] the conclusion of microscopic chaos using data from a Brownian motion experiment was based on a slightly different method of Cohen and Procaccia [3]. Both methods are clearly reviewed in Ref. [9].

We consider these methods as applied to the calculation of the KS entropy K , the non-zero value of which characterizes chaos. We recall the discussion of section III B where we concluded that the wind-tree models all have zero KS entropy, but the Lorentz gas has a KS entropy equal to its positive Lyapunov exponent.

The original Grassberger-Procaccia method [4] computes a slightly different dynamical entropy K_2 (defined using the square of the probability, p^2 rather than the conventional $p \log p$) satisfying the inequality $K_2 < K$. Thus a positive estimate $K_2 > 0$ implies that $K > 0$ and hence chaoticity. We follow Ref. [1] in using an adaptation due to Cohen and Procaccia [3] that allows K to be estimated directly.

We replace the experimental time series of the positions of the Brownian particle in Ref. [1] by a numerical time series of any of our infinite or periodic diffusive models, containing the x and y positions of the particle at 10^6 times uniformly spaced by a separation Δt . Unlike Ref. [1],⁷ our values of Δt , equal to 1 and 0.01 time units are close to the dynamical time scale determined by the mean free time $\bar{\tau}$ (see Sec. III A).

A single point on our numerical trajectory is denoted (x_i, y_i) , where i is an integer ranging from 0 to $10^6 - 1$. For the fixed oriented square (F) models the trajectory contains all the phase space information except the velocity which can take only four values in this case. For the randomly oriented square (R) and the Lorentz (L) models the velocity has one continuous degree of freedom. The Brownian motion experiment uses only one component (say, x) of the particle position, ignoring the huge number of other degrees of freedom contained in the fluid system. From a mathematical point of view, as long as the degrees of freedom are all coupled (that is, all the degrees of freedom depend on each other directly or indirectly), this type of method usually converges to the correct entropy (or dimension) using as few as one measured variable, however the efficiency may then well be such that an unreasonably large number of data points is required for a reliable estimate of these quantities.

A number (typically 10^2 to 10^3) of (in our case non-overlapping) uniformly spaced subsequences of the long trajectory are denoted “reference segments” (“reference trajectories” in Ref. [1]), having lengths n ranging from 1 to 100. These reference segments are compared with all subsequences of the trajectory having the same length. The comparison is made according to the position relative to the initial point of each subsequence, with a Euclidean metric in real space and a maximum metric over the trajectory. Thus, if i and j give the positions in the full trajectory of the initial points of the M reference segments and $N \approx 10^6$ total segments respectively, the distance between the segments beginning at i and j is defined as

$$d_n(i, j) = \max_{k=0}^{n-1} \sqrt{(\Delta x_{i+k} - \Delta x_{j+k})^2 + (\Delta y_{i+k} - \Delta y_{j+k})^2} \quad (9)$$

where $\Delta x_{i+k} = x_{i+k} - x_i$ etc.

We are now in a position to count the number of recurrences, in what is called “pattern probability” in [1]. For a given tolerance or spatial resolution ϵ we can define the probability of a certain pattern defined by the reference sequence beginning at i as the proportion of all the subsequences of the full trajectory that are within a distance (as defined above) ϵ of the reference sequence:

$$P(i, n, \epsilon, \Delta t) = \frac{1}{N} \#_j [d_n(i, j) < \epsilon] \quad (10)$$

and from this the “pattern entropy”

⁷Because there is only one experimental time series in Ref. [1], the authors generated new time series with time steps equal to a multiple of Δt by removing data points. The new time step was denoted τ . We do not need to do this in our numerical work, and we do not use the notation τ for time steps to avoid confusion with the mean free time.

$$K(n, \epsilon, \Delta t) = -\frac{1}{M} \sum_i \log_{10} P(i, n, \epsilon, \Delta t) \quad (11)$$

which gives the information theoretic entropy of the dynamics with respect to the pattern (of length n and resolution ϵ) probability distribution. The pattern entropy thus contains information about the n -time (displacement) distribution functions, as suggested by the discussion at the end of the previous section.

When the pattern entropy increases linearly with time in the limit of large n , it is possible to define an entropy per unit time,

$$h(\epsilon, \Delta t) = \frac{1}{\tau} \lim_{n \rightarrow \infty} [K(n+1, \epsilon, \Delta t) - K(n, \epsilon, \Delta t)] \quad (12)$$

In practice n is finite, and K is always bounded above by $\log_{10} N$ (since it is an average of $-\log_{10} P$, where P bounded below by $1/N$) and tends to saturate towards this value at long times. However, we can often find a large enough linear region in a plot of K as a function of n (for fixed ϵ and Δt) to compute $h(\epsilon, \Delta t)$. In Ref. [1] $h(\epsilon, \Delta t)$ was plotted as a function of ϵ with different curves corresponding to different Δt . From dimensional arguments it follows that any diffusive process has a scale invariance leading to a dependence $h \sim 1/\epsilon^2$, which is in fact observed in such plots.

Assuming that there is sufficient data that all the limits (of large N , M and n) can be approximated reliably, the KS entropy K is equal to the maximum value of $h(\epsilon, \Delta t)$ as ϵ and Δt are varied. The measured value $h(\epsilon, \Delta t)$ will be less than the true KS entropy K if the values of ϵ and or Δt are so large that not all of the information contained in the dynamics is represented in the time series. This effect does not explain why a nonchaotic system may appear to be chaotic, that is, why the measured value of $h(\epsilon, \Delta t)$ is greater than $K = 0$, as in Ref. [2]: this must be due to a problem with the above mentioned limits, and we defer a discussion of this point until after we have presented our results.

Our results for each of the six models [F,R,L][∞ ,P4] are illustrated in Fig. 8 with $\Delta t = 1$ and in Fig. 9 with $\Delta t = 0.01$. The case $\Delta t = 1$ samples the motion of the particle as it begins to diffuse among the scatterers. The models (both chaotic and nonchaotic) are indistinguishable, with the linear growth of the pattern entropy suggesting positive KS entropy, except that the superdiffusive model FP4 is showing signs that the KS entropy is zero, as a nonchaotic model should.

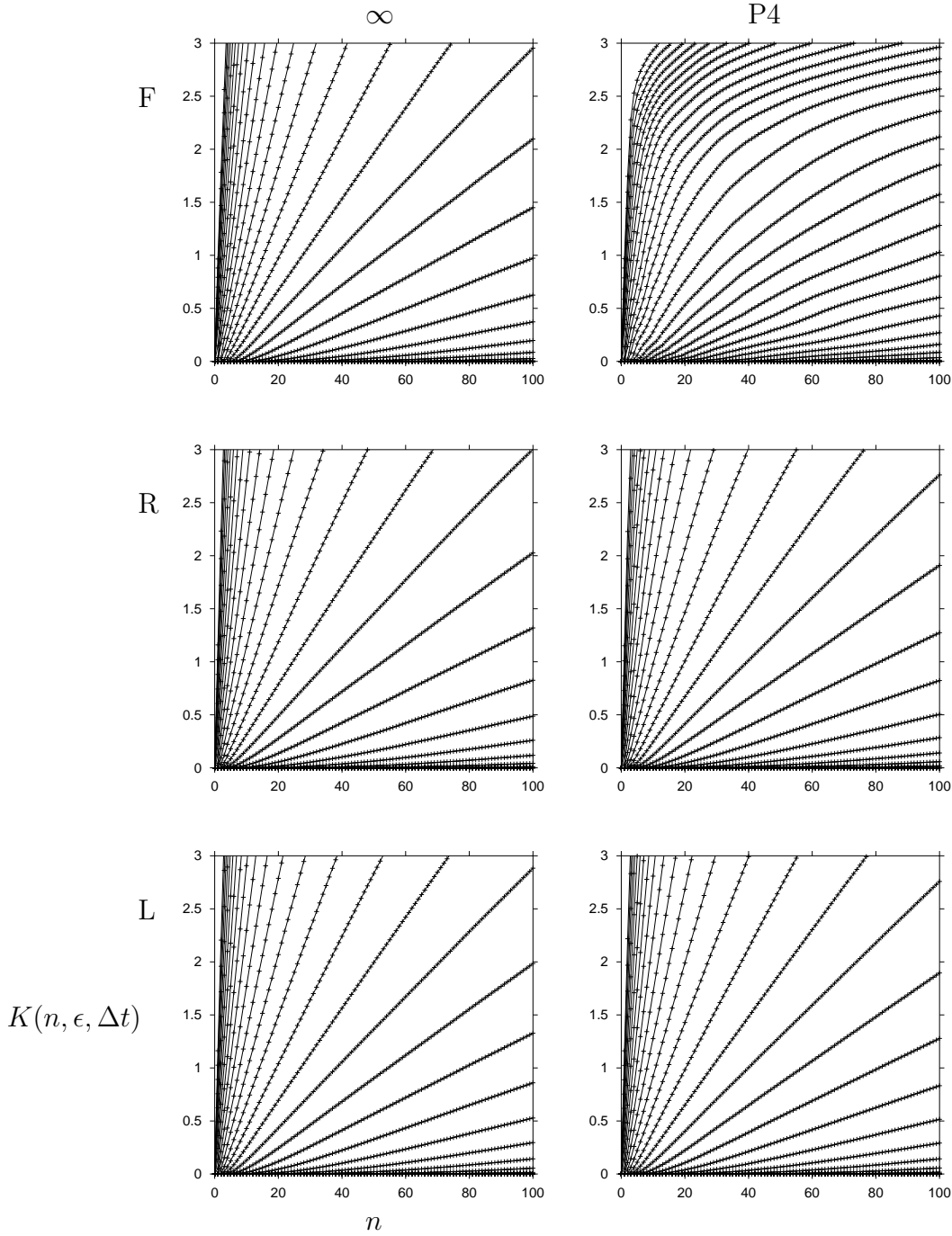


FIG. 8. The pattern entropy $K(n, \epsilon, \Delta t)$, Eq. (11), plotted against the segment length n for a time step $\tau = 1$. The models (see Sec. II C) are F (upper), R (middle) and L (lower), each with ∞ (left) and $P4$ (right). The different curves on each graph correspond to different values of ϵ from approximately 0.3 to 300 in multiples of 1.21; large values of ϵ correspond to smaller pattern entropies since the probability of recurrences $P(i, n, \epsilon, \tau)$ is then larger. A linear behavior indicates positive KS entropy, so both chaotic and nonchaotic models appear to be chaotic except the superdiffusive model FP4; see the discussion in the text.

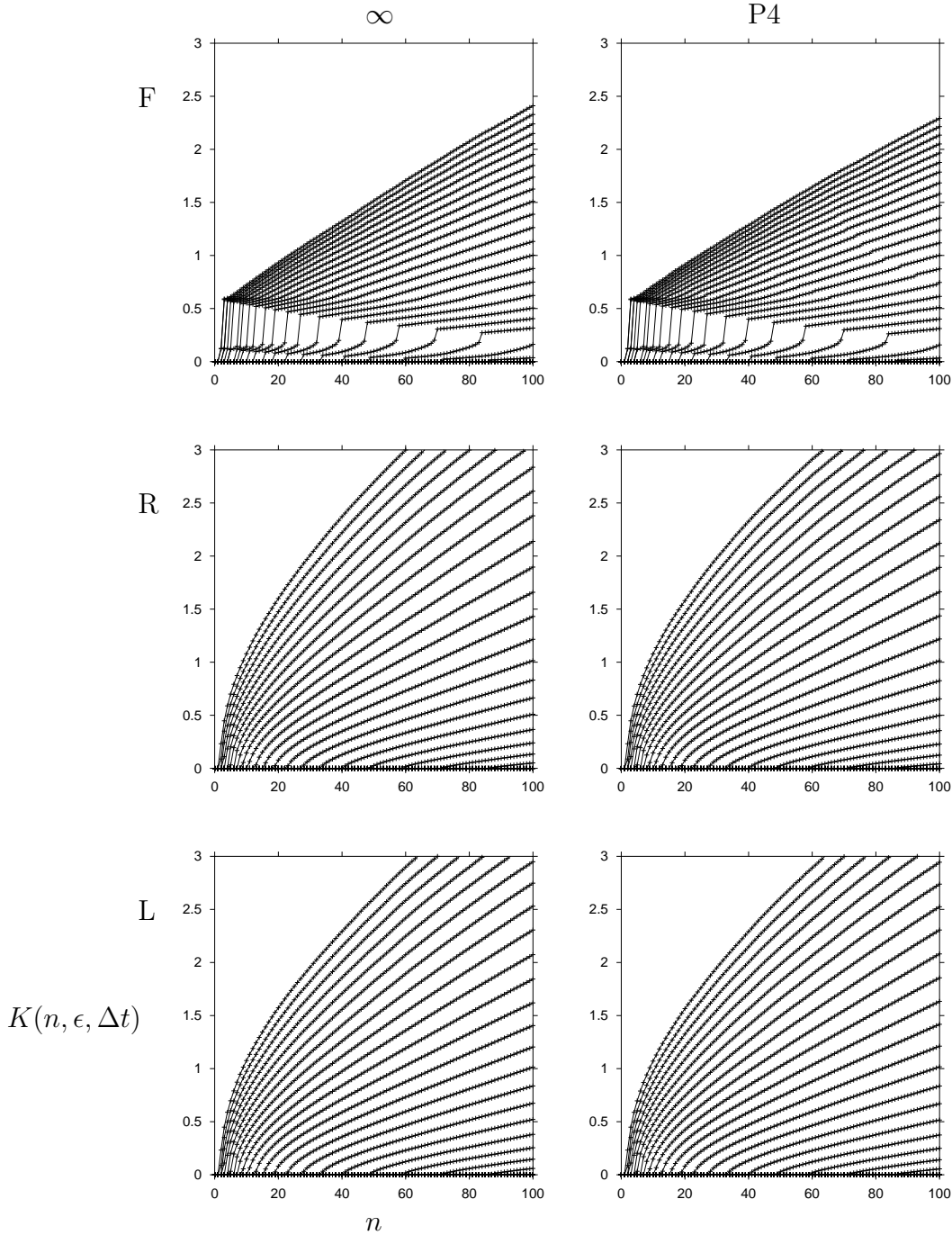


FIG. 9. The pattern entropy $K(n, \epsilon, \Delta t)$, Eq. (11), plotted against the segment length n for a time step $\Delta t = 0.01$. See Fig. 8 for details, except that the range of ϵ is now approximately 0.03 to 30. At short times, the trajectories are mostly uninterrupted straight lines, and hence do not appear chaotic; the lines curve with decreasing gradient. At longer times, there are some collisions, leading to a straightening (more chaotic behavior). The chaotic and nonchaotic models look the same, as in Fig. 8 except that the particle in the F models has only four velocity directions, leading to the characteristic feature below an entropy equal to $\log_{10} 4 \approx 0.6$.

For $\Delta t = 0.01$ (Fig. 9), where mostly ballistic behavior occurs, the graphs of pattern entropy vs. number of time steps is no longer linear. The R and L models look much the same, while the F models have an unusual feature when the pattern entropy is equal to $\log_{10} 4 \approx 0.6$ which is due to the four available wind directions, that is, only a fourth of the trajectories at a given (x, y) point are close in phase space after a certain time. The pattern entropy is becoming linear at larger times

in all models, suggesting positive KS entropy.

We can draw the following conclusions about the use of Grassberger-Procaccia type methods for this class of problems: (a) measurements need to be made at microscopic time scales, (b) even at microscopic time scales, the method does not seem to distinguish between chaotic and nonchaotic dynamics, and (c) the reason seems to be that unfeasibly long time series are needed in order to do that.

Macroscopic measurements It is clear that in an analysis as explained above, using large distance and time scales a diffusive system shows itself as almost independent of its microscopic dynamics (whether chaotic, non-chaotic or stochastic), although we cannot exclude the possibility that an unreasonably long trajectory might still give some evidence of weak correlations that survive for macroscopic times. In the Brownian motion experiment, for example, there are of the order of 10^{10} collisions of the Brownian particle with the surrounding solvent between each measurement of its position, so any correlations arising from, say, nonchaotic microscopic dynamics would be effectively averaged out between measurements. This is essential from the point of view of designing future experiments, but it is not the full story as it does not explain our results, which are obtained using short times. The Brownian motion experiment could not investigate the motion at short time scales, but it is important to know whether data from an improved experiment might determine the microscopic chaoticity in principle.

Microscopic measurements Our results do not suggest that the Grassberger-Procaccia type methods can distinguish between chaotic and nonchaotic diffusive models even at short times because the nonchaotic R models consistently give the same results as the chaotic L models. The only distinctions we have been able to make are between diffusion and superdiffusion for $\Delta t = 1$, and between the continuous velocity space of the R and L models and the four velocity directions of the F models. Both of these distinctions can be made from a time series without using the intensive analysis of the Grassberger-Procaccia method.

How long a time series is required? Our wind-tree models appear unpredictable (in the sense of positive KS entropy) because it takes the system some time to “realize” that it is nonchaotic, in other words, quite a long time series length N is required. For example, the most pronounced nonchaotic diffusive model we have is RP4. Once the particle “knows” the positions and orientations of all the scatterers, the system is completely predictable, and hence a zero KS entropy is manifest. How long does it take the particle to determine the positions and orientations of the scatterers? For that the particle must at least collide with two adjacent sides of each of the 4 scatterers, a total of 8 collisions. It typically takes 14 collisions to accomplish this, with approximately 6 possible sides at each collision, that is a total of roughly $6^{14} \approx 10^{11}$ ways for the particle to obtain the positions of all the scatterers. It is clear that our analysis of a trajectory of length 10^6 cannot hope to enumerate all these possibilities, let alone obtain sufficient statistics on the probabilities of each of them. For the infinite models such as R_∞ the motion of the particle is never completely predictable, but the proportion of collisions that the particle encounters new scatterers decreases as $1/\log t$ according to the discussion of Sec. III B. The measurement of such a slow decrease is far beyond the capabilities of any feasible implementation of the Grassberger-Procaccia method.

Since the Grassberger-Procaccia approach does not seem to distinguish our chaotic and non-chaotic diffusive models, we turn to an alternative time series analysis method, with a view towards suggesting possible methods for analyzing future experiments that are able to sample the dynamics on microscopic time scales. Such a method cannot possibly enumerate all possible trajectory segments, as discussed above, but there are certain types of trajectory segments, namely those that are almost periodic, that stand out as predictable in a nonchaotic system. The method of the next section takes advantage of this property, and in effect distinguishes chaotic and nonchaotic systems by singling out this subset of all possible recurrences.

V. ALMOST PERIODIC RECURRENCES

A. Motivation

We have seen in Sec. IV that the variant of the Grassberger-Procaccia method used by Gaspard et al cannot distinguish between nonchaotic and chaotic models, for the reason that the time series (either experimental or numerical) is not long enough to provide a reasonable approximation to the infinite time limit implied by the method.

We can attempt to circumvent this difficulty by looking for specific types of recurrences, as opposed to taking an average over all types of recurring trajectory segments. In particular we will

show that a promising candidate for a useful specific recurrence is given by one that corresponds to an orbit that is almost periodic (again, within a spatial tolerance ϵ). We can identify these almost periodic orbits as those that repeat (within a distance ϵ) their previous motion at equally spaced intervals of time, hence the name “Almost periodic recurrences” (APR).

If we compare the APR approach with the Grassberger-Procaccia (GP) method, there are a number of similarities and differences. Both methods are designed to deduce chaotic properties from time series data. GP aims to make quantitative statements about the KS entropy, whereas APR as yet only provides a qualitative statement about chaoticity. Both methods make use of the probability of events that recur. GP then averages over these probabilities, while APR singles out especially significant events. This means, for example that in an intermittent system, where the dynamics switches irregularly from chaotic to regular behavior, GP measures only the average, chaotic, dynamics, while APR is sensitive to the lack of chaoticity in the regular regions of phase space.

We now discuss the properties of periodic orbits in chaotic and nonchaotic systems (particularly our models), before describing the APR method in more detail and presenting the results.

B. Periodic orbits in chaotic systems

Periodic orbits are of great importance in chaotic systems. Although typical trajectories (as defined by the Liouville or natural measures) are not periodic, there are many systems for which they are approximated by periodic orbits when the periodic orbits are dense in the phase space or on an attractor. This allows many properties to be computed from expansions involving periodic orbits [16].

The properties of the periodic orbits are not directly related to the other chaotic properties discussed in Sec. IIIB, yet they do tend to differ between chaotic and nonchaotic systems, and so they constitute additional chaotic properties. The properties of the periodic orbits in the Lorentz gas are of most interest to us, and in some sense typical for chaotic systems, so we focus on these. In this and the following section we examine two relevant properties of periodic orbits, and sketch proofs of these properties.

Existence There is an easy constructive proof of the existence of periodic orbits in the Lorentz gas: Choose two disks arbitrarily; the line joining their centers gives a periodic orbit unless there is a disk interposing; consider one of the original disks and the interposing disk, and repeat until no disk interposes.

Stability The periodic orbits are exponentially unstable, that is, almost all trajectories beginning a small distance ϵ from the periodic orbit at time $t = 0$ are at a distance $\epsilon e^{\lambda_p t}$ at time t , where λ_p is the maximum (here the only positive) Lyapunov exponent, which depends on the periodic orbit p . This exponential instability makes it very unlikely for a typical trajectory to remain near a given periodic orbit for long times.

C. Periodic orbits in nonchaotic systems

We study here the properties of periodic orbits of our wind-tree models, which are typical of nonchaotic systems, without attempting to classify all possible nonchaotic periodic behavior. For a complementary study of the periodic orbits in polygonal billiards, see Ref. [17].

Not all wind-tree models have periodic orbits. The argument given above for the Lorentz gas fails because an orbit connecting two square scatterers is periodic only if the scatterers have the same orientation (of zero probability in the randomly oriented model) and the particle moves perpendicular to the surface of the scatterers (excluded by definition in the fixed orientation model). In general, the existence of periodic orbits depends on the locations and orientations of the scatterers. We will find that using generic locations of scatterers periodic orbits exist in the R_∞ model, but not in the F_∞ model. The periodic models (such as FP4 and RP4) are harder to treat mathematically, and are not discussed here.

F model: nonexistence The absence of periodic orbits for generic configurations of the F_∞ model follows directly from arguments in a proof of Aarnes [18]. In order for the particle to return to its starting point, an expression linear in the positions of the scatterers must vanish. The coefficients of the (x, y) position of a scatterer in this expression are integers depending on which faces the particle hits, and are zero only if the particle hits opposite faces an equal number of times. A simple

reductio ad absurdum argument shows then that there is a scatterer (perhaps more than one), the furthest to the top and right (largest value of $x + y$), which has collisions on only one of its faces (the lower left), and hence the coefficients corresponding to the position of this scatterer are nonzero. If the scatterers are randomly placed, no linear combination of the positions can vanish, so no periodic orbit can exist. Of course, there are special configurations of the scatterers (such as at the corners of a square aligned with the coordinate axes) that allow periodic orbits. Since there are therefore generically no periodic orbits in the F_∞ model, the remainder of this section refers to the R_∞ model.

R model: existence The existence of periodic orbits for generic configurations of the R_∞ model follows from the observation that any set of configurations of a finite number of (*eg.* 3) scatterers with nonzero (Lebesgue) measure includes configurations appearing somewhere in a generic infinite configuration. A period 3 orbit can always be found in an acute triangular billiard by minimizing the total path length, see Fig. 10. If three scatterers outline an acute triangle and are positioned so that their faces contain the path of minimal length (clearly of nonzero measure), a period 3 orbit exists.

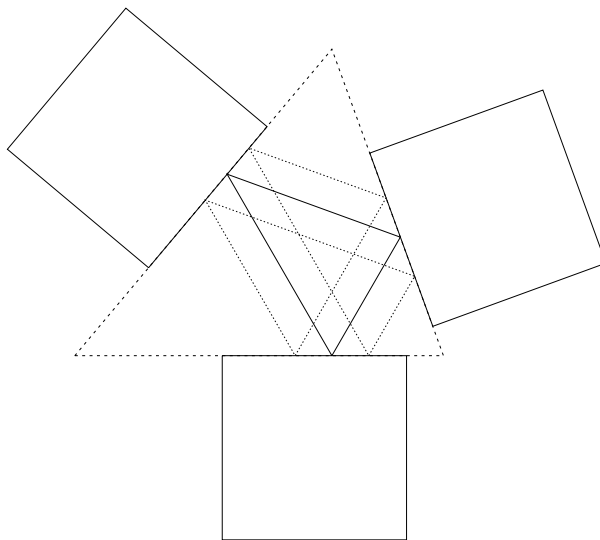


FIG. 10. Construction of periodic orbits in the infinite randomly oriented wind-tree model R_∞ . Any acute angled triangle (dashed), generated by three scatterers (solid squares), contains a period 3 orbit of minimal length (solid triangle). It is surrounded by a family of period 6 orbits (dotted) that differ from the period 3 orbit by the location of the collisions but not the direction of the velocities.

R model: stability Finally we investigate the stability of periodic orbits in the R_∞ model. The combination of the linear dynamics of the free particle with length preserving reflections leads to a linear separation of nearby trajectories. That is, an initial separation of ϵ in the direction of the velocity leads to a separation ϵt in the position after time t . Another way of saying this is that the number of uniformly distributed trajectories remaining within a distance ϵ of the periodic orbit is ϵ/t for large t . Thus a particle in the R_∞ model is quite likely to spend a long time near a periodic orbit, in contrast to in the Lorentz gas.

D. Details and results

Now we return to our method of Almost Periodic Recurrences for distinguishing chaotic properties of diffusive systems from a time series. This consists of counting the number of almost periodic

sequences in the time series, thus hoping to exploit the different properties of periodic orbits in chaotic and nonchaotic systems as discussed in the previous two sections.

As in the Grassberger-Procaccia method we begin with a time series containing 10^6 positions of the particle (x_i, y_i) spaced at a time interval $\Delta t = 1$, see Sec. III A. Analogous to Eq. (9) we define a distance between two segments of length T (the period of an almost periodic orbit) that begin at points i and j on the trajectory,

$$d_T(i, j) = \max_{k=0}^{T-1} \sqrt{(x_{i+k} - x_{j+k})^2 + (y_{i+k} - y_{j+k})^2} \quad (13)$$

Using Eq. (13) we compute the number of initial points i for which the orbit repeats within a tolerance ϵ ,

$$N_T(i) = \#_i[d_T(i, i+T) < \epsilon] \quad (14)$$

where we use $\epsilon = 1$ for the results presented in Fig. 11.

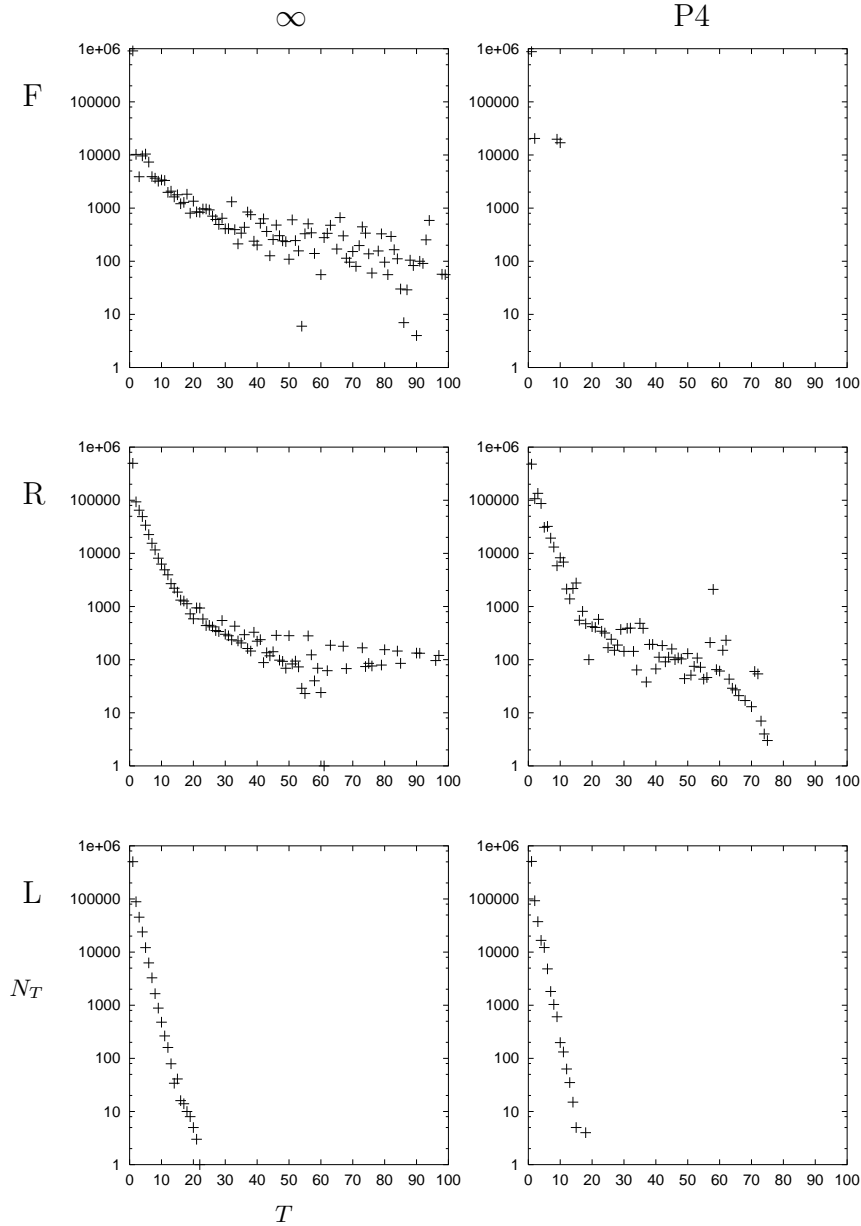


FIG. 11. Results of the APR method, showing the number of times in which a periodic orbit of a given length T was repeated within a tolerance $\epsilon = 1$. The models (see Sec. II C) are F (upper), R (middle) and L (lower), each with ∞ (left) and P4 (right). The chaotic Lorentz models show a clear exponential decrease with T , while the nonchaotic models exhibit distinctly different behavior depending on the properties of their (almost) periodic orbits; see the text.

It is clear that the chaotic Lorentz models, with an exponential decay of N_T with T can be easily distinguished from the nonchaotic F and R models which mostly have a slower and noisier decay, so we have achieved our objective of finding a time series analysis method that can distinguish between time series of chaotic and nonchaotic diffusive systems. It remains for us to explain the difference, and the plots obtained using the properties of the periodic orbits in these systems. For that, we note that there are two types of (almost) periodic orbits that might appear in the expression for N_T : An orbit of length T that has been (almost) repeated, and a shorter orbit of length T/n that has appeared $2n$ times, so that the total time is equal to $2T$.

The L models In the Lorentz gas, the probability of remaining near a periodic orbit for a time T is of order $e^{-\lambda_p T}$ (see Sec. V B), where λ_p is the maximum (here the only) positive Lyapunov exponent, and depends on the periodic orbit p . This is why both the infinite and periodic Lorentz gases give an exponential form in Fig. 11. Because N_T can be due to long orbits or repeats of short orbits, the exponential form depends on both (1) the exponential escape from short orbits with many repetitions and (2) the exponential instability of orbits with length, that is, that λ_p does not approach zero for long orbits.⁸

The R models In the randomly oriented wind-tree models, the probability of remaining near a periodic orbit for a time T is of order $1/T$ (see Sec. V C). This form is not immediately apparent in Fig. 11 because orbits (particularly those surviving for long times) can be counted more than once due to contributions from an interval of different initial points i . Both the $R\infty$ model and the RP4 model continue beyond $T = 100$ due to increasingly rare long orbits and many repeats of shorter orbits. For example, the almost periodic orbit giving rise to the conspicuous point with period $T = 58$ in the RP4 model is repeated many times, also contributing to multiples of the period, double $T = 114, 115$; triple $T = 172, 173$; and so on up to $T = 1033, 1034$. It is clear that the dynamics is completely different to that of a chaotic system.

The F models In the fixed oriented wind-tree models, there are no periodic orbits (see Sec. V C). This means that any contribution to N_T is due to orbits that are close to periodic. The infinite model $F\infty$ contains many arrangements of a few scatterers that come arbitrarily close to generating a true periodic orbit, so the plot is similar to that of the R models. The periodic model FP4, in contrast, has only a few short orbits that are at all close to periodic, and none that can be repeated to give further contributions at higher values of T , or these would be observed in the figure.

What we have presented here barely scratches the surface of the Almost Periodic Recurrences method and its variants. It would be quite easy to search for 3 or more occurrences of an (almost) periodic orbit, or to distinguish between a single repeat of a long orbit and many repeats of a short orbit. We have restricted the presentation here to a demonstration of the method as a means to distinguish time series of chaotic and nonchaotic diffusive systems, but we hope that it will be useful in more general contexts.

VI. ABSORBING BOUNDARY CONDITIONS

The case of absorbing boundary conditions provides a rich context for illuminating the differences between chaotic and nonchaotic diffusion. This is because the diffusion equation with absorbing boundary conditions leads naturally to an exponential escape process, while the periodic orbits of the randomly oriented wind-tree model require a power law escape process (see Sec. V C), thus violating the diffusion equation.

We consider here the probability that a single randomly placed particle will remain in an open system⁹ for a given time, or equivalently, the number of identical noninteracting particles remaining in the system after the same time. For chaotic dynamics the escape rate formalism of Gaspard and

⁸ There is a minor technical difficulty associated with the random Lorentz gas: It is possible due to the random placement of the scatterers to have arbitrarily long free paths between collisions, leading to the possibility that λ_p could become arbitrarily small. However, the probability of a long free path is also exponentially small, so the result is still exponential.

⁹We describe systems with absorbing boundaries as “open”.

Nicolis [7,19,20] uses the escape rate (defined below) to connect the diffusion coefficient to dynamical properties such as the KS entropy and the positive Lyapunov exponents. For nonchaotic systems the escape process is qualitatively different depending on the properties of the periodic orbits as we have noted above, and the escape rate formalism must be generalized, if it is to make any sense at all. We now describe the escape rate formalism as it applies to chaotic systems, discuss the results for our models, and then attempt to generalize the formalism to include nonchaotic systems.

A macroscopic description of escape on a square (for simplicity; other geometries are analogous) is given by the diffusion equation (1) for the particle density $P(\mathbf{x}, t)$, together with the boundary condition $P = 0$ along the lines $x = 0$, $y = 0$, $x = L$ and $y = L$. The general solution is

$$P(\mathbf{x}, t) = \sum_{m,n=1}^{\infty} a_{m,n} \sin(m\pi x/L) \sin(n\pi y/L) e^{-\gamma_{m,n} t} \quad (15)$$

with the decay rate

$$\gamma_{m,n} = \frac{D\pi^2}{L^2} (m^2 + n^2) \quad (16)$$

At long times, the solution is dominated by the slowest decaying mode, corresponding to the escape rate

$$\gamma = \gamma_{1,1} = \frac{2D\pi^2}{L^2} \quad (17)$$

Note that the escape of particles is exponential in (15). The escape rate formalism equates this macroscopic escape rate γ with the (exponential) escape rate of a (microscopically) chaotic system, which is related to its KS entropy K and the sum of its positive Lyapunov exponents $\sum \lambda_+$ (here at most a single positive Lyapunov exponent) by [9]

$$\gamma = \sum \lambda_+ - K \quad (18)$$

the “escape rate formula” which generalizes Pesin’s formula (Sec. III B) to open systems. Not only can the escape rate of chaotic systems be calculated from periodic orbit theory [16], but, as we will show below, there is an intimate connection between periodic orbits and the escape process in nonchaotic systems.

We now present our numerical results, from which we learn how the above theory for chaotic systems is modified in the nonchaotic case. As described in Sec. II B, the arrangement of scatterers used is the same as in the periodic case with $L = 20$; the absorbing boundaries are one distance unit from the edge of the periodic cell, leading to an open system of size $L = 18$. As before we use fixed oriented squares (F), randomly oriented squares (R) or circles (L). We denote absorbing boundary conditions by A, so the full notation for these models is [F,R,L]A18. We place 10^7 particles uniformly (without overlapping the scatterers) in the square of size $L = 18$ and compute the number of particles remaining in the system as a function of time, see Figs. 12, 13.

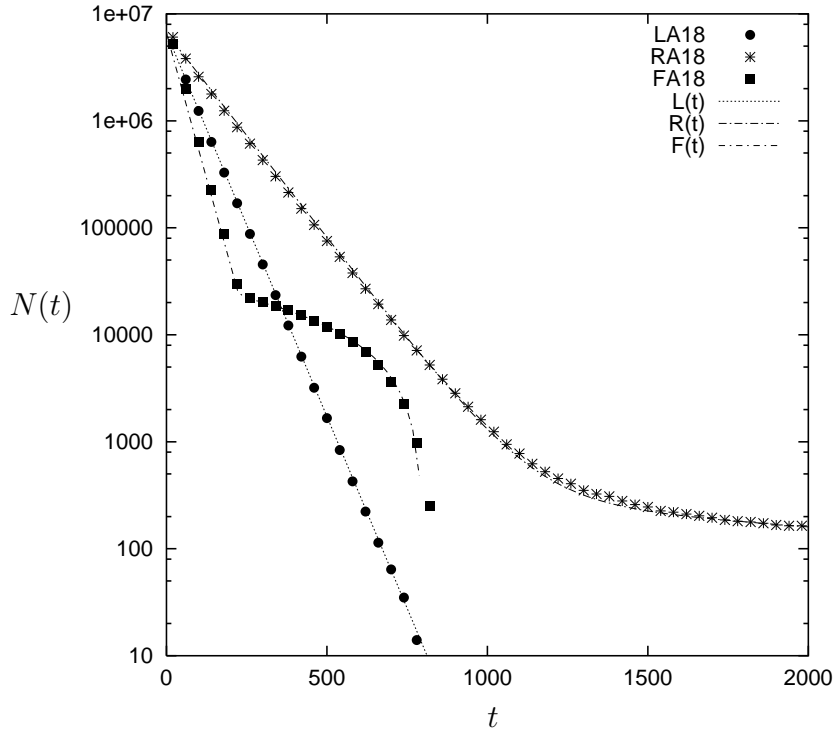


FIG. 12. The decay of the number of particles with time when the boundaries are absorbing for the Lorentz gas LA18 (circles), randomly oriented wind-tree model RA18 (stars) and the fixed oriented wind-tree model FA18 (squares). The decay is exponential for short times for all three models as predicted by the diffusion equation, and model-dependent for long times. The LA18 model remains exponential, while the RA18 model switches to a $1/t$ form and the FA18 model switches to a linear $t_c - t$ form. The results are well described by the functions $L(t)$, $R(t)$ and $F(t)$ respectively, see Eqs. (19-21)

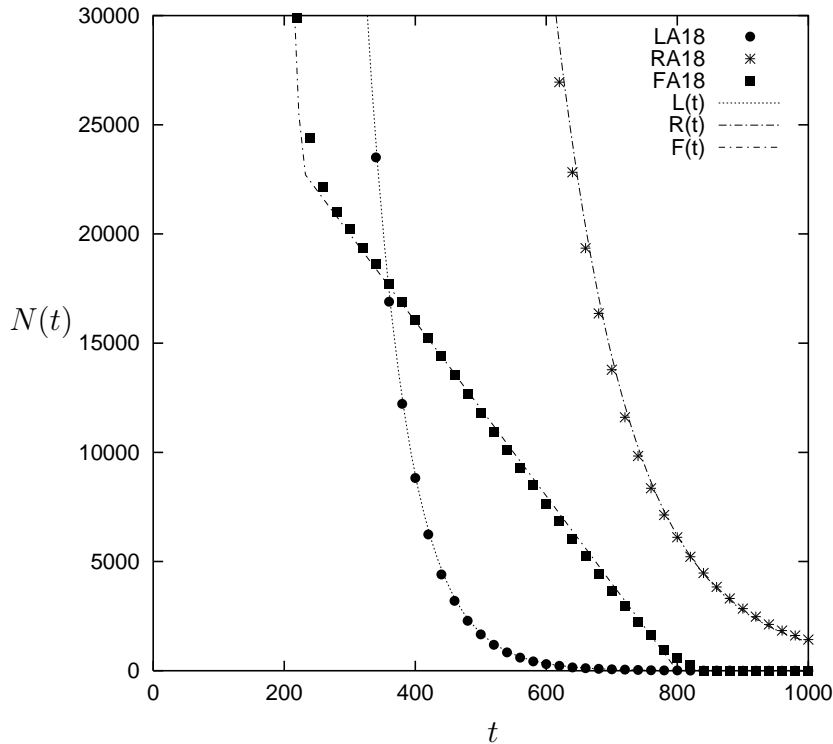


FIG. 13. Fig. 12 plotted with a linear vertical axis to show the linear form of the escape in the FA18 model.

The chaotic Lorentz gas exhibits exponential decay as predicted by the diffusion equation for all times, but the nonchaotic wind-tree models deviate from exponential decay at late times. The results are well described by the empirical expressions

$$L(t) = 6.6 \times 10^6 \times e^{-0.0165t} \quad (19)$$

$$R(t) = 6.6 \times 10^6 \times e^{-0.0088t} + 3.2 \times 10^5/t \quad (20)$$

$$F(t) = \begin{cases} 6.6 \times 10^6 \times e^{-0.025t} & t < 226 \\ 40(800 - t) & 226 < t < 800 \\ 0 & t > 800 \end{cases} \quad (21)$$

for the L, R and F models respectively over the range of times considered. The initial exponential decay may be compared with Eqs. (15-17) to give an effective diffusion coefficient. We find $D_L = 0.27$, $D_R = 0.14$ and $D_F = 0.41$, which are certainly consistent with the results of the mean square displacement, Tab. I in Sec. III C, given that Eqs. (15-17) depend on the macroscopic diffusion equations, and so requires a large system $L \rightarrow \infty$ limit. The coefficient 6.6×10^6 is obtained by matching Eq. (15) to the uniform probability density of the initial conditions; this comes to $64N(0)/\pi^4$ with $N(0) = 10^7$ as the initial number of particles in the system. From this close agreement, we conclude that the early escape is well described by the diffusion equation with the same diffusion coefficient that appears in the mean square displacement of Sec. III C; there is no trace of non-diffusive behavior at short times.

The R model We now discuss the long time behavior of the nonchaotic models. The randomly oriented wind-tree model has a $1/t$ decay in (20) due to its periodic orbits; particles that are initially close to a periodic orbit lead to this power law as described in Sec. V C. The coefficient gives an estimate of the density of periodic orbits; 3.2×10^5 is quite small compared to the number of particles, 10^7 , so periodic orbits are relatively rare in a sense that is difficult to define precisely. In terms of the escape rate formalism, a power law decay corresponds to an escape rate $\gamma = 0$ which trivially satisfies (18), but yields no information about the diffusion coefficient D , that is, (17) is not satisfied.

The F model The fixed oriented wind-tree model shows a complete escape of all the particles in a finite time, as might be expected from the lack of periodic orbits. The dramatic transition from

many independent particles, and taking the limit of an infinite number of particles.

We can, however, attempt to calculate the diffusion coefficient in the finite wind-tree models by taking the $t \rightarrow \infty$ limit at the same time as the $L \rightarrow \infty$ limit. This is because the diffusion equation is a good approximation even in the open case as long as the time is not too long, and the decay remains exponential. For example, assuming that the “density of periodic orbits” in the RA model is independent of L (which seems to be the case numerically), the transition time from exponential to power law decay, as determined by comparing the two terms in Eq. (20) using Eq. (17) is of order $t_{tr} \approx L^2 \log L$. This should be compared with the time scale for which the slowest decaying mode of the diffusion equation dominates, $t_D \approx L^2$, see (16). Thus, for a given L , there is a narrow range in time $t_D \ll t \ll t_{tr}$ in which the decay is exponential, and in which a limit can be taken to obtain D from the escape process. For example we can combine the L and t limits by setting $L = u$ and $t = u^2 \sqrt{\log u}$,

$$D = \frac{1}{2\pi^2} \lim_{u \rightarrow \infty} \frac{1}{\sqrt{\log u}} \ln \frac{P_u(u^2 \sqrt{\log u})}{P_u(0)} \quad (23)$$

We expect this relation to hold for all the models [L,R,F]A. We emphasize that Eq. (23), if it is mathematically valid, still does not provide a practical method for computing the diffusion coefficient beyond the estimates we gave following Eq. (21). This is because the range of time scales $t_D \ll t \ll t_{tr}$ grows so slowly with L that extremely large system sizes are required for more precise estimates of D .

We can also turn the argument around, and suggest that the escape at long times of finite systems may be a good experimental technique for detecting (or ruling out at some level) nonchaotic microscopic dynamics. In any case, the range of validity of the diffusion equation as a macroscopic description of nonchaotic systems is restricted.

VII. DISCUSSION AND OPEN QUESTIONS

We have explored the connections between microscopic chaos and diffusion. On a superficial level, the details of the microscopic dynamics seem to have little effect on the diffusion process: Gaussian diffusion is observed in our RP4 model, which has scatterers with flat sides (hence no exponential separation of nearby trajectories) and is periodic (hence there is no source of randomness from a disordered environment). In addition, the Grassberger-Procaccia method of time series analysis cannot distinguish our chaotic and nonchaotic diffusive models because it would require impractically long data sets. On a deeper level, however, the subtle differences between chaotic and nonchaotic diffusion are quite apparent if you know where to look: Our time series analysis method based on periodic orbits has no trouble distinguishing between the chaotic and nonchaotic models, and the long time behavior of escape from an open system is also determined by the properties of the chaotic versus nonchaotic periodic orbits.

In the light of our results, we can make a few concrete suggestions for an experimental determination of the chaotic or nonchaotic properties in a diffusive system. Firstly, as we remarked in Ref. [2], it is necessary to make measurements on the distance and time scales relevant to the microscopic dynamics. In our models, this question is simplified by the fact that all microscopic time scales are of order one in our units, Sec. III A. Once this is achieved, one could use an approach based on the method of Almost Periodic Recurrences, which searches for periodic behavior; alternatively the late time decay of particles from an open system can also elicit the chaotic or nonchaotic nature of the dynamics.

We conclude with some open questions and possibilities for further work. In terms of *microscopic chaos*, we have studied only a few models. We note that there are examples of lack of chaoticity we have not considered, such as the coexistence of chaotic and nonchaotic regions found in KAM theory. In terms of *diffusion*, we note that in the light of Sec. VI the diffusion equation is not a complete macroscopic description of nonchaotic diffusion. In terms of *time series analysis*, our APR method, while sufficient for our purposes here, could be much more developed and applied. With regard to *periodic orbit theory*, the methods developed for exploiting the importance of periodic orbits to compute properties of chaotic systems [16] do not apply to nonchaotic systems, and yet we have seen that periodic orbits also play an important role in nonchaotic systems.

We note that our infinite models, while sharing some of the properties of corresponding finite billiards, appear to fall outside the domain of current mathematics. For example, a recent study of infinite billiard systems [21] is mostly restricted to cases with finite areas that are finitely connected; our models obey neither of these conditions. It would be interesting to see if it is possible to

rigorously determine the status of our models, particularly their ergodic properties, rate of decay of correlations and Kolmogorov-Sinai entropy within the framework of some mathematical theory of infinite nonchaotic systems. More generally, a mathematical understanding of statistical mechanics including the thermodynamic limit naturally leads to the study of infinite systems.

Finally, we remark that all the models we have considered — with the exception of one (FP4) — are diffusive, limiting our investigation as to the presence of microscopic chaos or not to such systems. In addition, the precise role played by microscopic chaos — as represented by the Lyapunov exponents — and “macroscopic chaos”, as embodied by the randomly placed scatterers for the existence of a diffusion process and the value of the diffusion coefficient, remains open. A similar but more complicated situation obtains when diffusion of momentum (viscosity) or energy (heat conduction) and other transport processes are considered.

ACKNOWLEDGMENTS

We thank L. Bunimovich, J. R. Dorfman, P. Gaspard and I. Procaccia for stimulating discussions. We are particularly indebted to H. van Beijeren for many very helpful discussions and suggestions. This work was supported by the Engineering Research Program of the Office of Basic Energy Sciences of the US Department of Energy under contract #DE-FG02-88-ER13847.

APPENDIX A: THE MEAN FREE TIME

We give here a calculation of the mean free time for our models quoted in Sec. III A. Our derivation is due to Chernov [22], extended to the fixed oriented model, and with a technical caveat for the infinite models. Refer to Sec. II B for the definitions of R , L , N and ρ .

The mean free time $\bar{\tau}$ is equal to the mean free path, since the velocity is one. The mean free time is known exactly for billiard systems [22], which include the [R,L]P models discussed here. We make a minor extension to allow the FP model (which differs because we do not want to allow all velocity directions). We expect that the formula for the mean free time would still hold in the infinite models on physical grounds, but we cannot justify this mathematically. Briefly, the argument in Ref. [22] observes that the total volume of phase space V can be computed in two different ways.

One expression for the volume of phase space is as an integral over the area of the billiard, giving $V = 4A$ for the original wind-tree model with fixed orientations, and $V = 2\pi A$ for random orientations or the Lorentz gas. Here, V is the volume of phase space, including both position and velocity, while A is the area accessible to the point particle. For our infinite billiards we think of a large but finite periodic system of length L , and formally take the limit $L \rightarrow \infty$ at the end of the calculation. Since the area A is equal to $L^2(1 - \rho)$, we have $A = L^2/2$ here as $\rho = 1/2$. The prefactor 4 comes from the four possible wind directions, and the 2π from integrating over all possible directions. Putting these expressions together we have $V = 4L^2(1 - \rho)$ for fixed oriented squares and $V = 2\pi L^2(1 - \rho)$ for randomly oriented squares or circles.

An alternative expression for the volume of phase space is an integral over the boundary of the billiard, where the contribution from each point is given by the free path/time τ . In this way we find $V = \sqrt{2}\bar{\tau}P$ for fixed oriented squares and $V = 2\bar{\tau}P$ for randomly oriented squares or circles. Here P is the length of the boundary, that is, the total perimeter of all the scatterers, $\bar{\tau}$ is the *mean* free path/time, and the numerical prefactor is the integral over the component of velocity perpendicular to the boundary. For the wind-tree models we have $P = 4\sqrt{2}N$ where N is the number of scatterers, so $P = 2\sqrt{2}\rho L^2$; for the Lorentz gas, we have $P = 2\pi RN = \sqrt{2\pi}\rho L^2$.

Comparing the expressions for V in both calculations, we find $\bar{\tau} = (1 - \rho)/\rho = 1$ (using our value of $\rho = 1/2$) for the case of fixed oriented squares, $\bar{\tau} = \pi(1 - \rho)/(2\sqrt{2}\rho) = \pi/(2\sqrt{2}) \approx 1.111$ for the case of random oriented squares, and $\bar{\tau} = \sqrt{\pi/2}(1 - \rho)/\rho = \sqrt{\pi/2} \approx 1.253$ for the Lorentz gas.

[1] P. Gaspard, M. E. Briggs, M. K. Francis, J. V. Sengers, R. W. Gammon, J. R. Dorfman, and R. V. Calabrese, *Nature* **394**, 865 (1998).

- [2] C. P. Dettmann, E. G. D. Cohen and H. van Beijeren, *Nature* **401**, 875 (1999).
- [3] A. Cohen and I. Procaccia, *Phys. Rev. A* **31**, 1872 (1985).
- [4] P. Grassberger and I. Procaccia, *Phys. Rev. A* **28**, 2591 (1983).
- [5] E. H. Hauge and E. G. D. Cohen, *J. Math. Phys.* **10**, 397 (1969).
- [6] H. van Beijeren, *Rev. Mod. Phys.* **54**, 195 (1982).
- [7] P. Gaspard, *Chaos, Scattering and Statistical Mechanics* (Cambridge University Press, Cambridge, 1998).
- [8] W. W. Wood and F. Lado, *J. Comp. Phys.* **7**, 528 (1971).
- [9] J.-P. Eckmann and D. Ruelle, *Rev. Mod. Phys.* **57**, 617 (1985).
- [10] L.-S. Young, *Ann. Math.* **147**, 585 (1998).
- [11] N. I. Chernov and C. P. Dettmann, *Physica A* (in press), [chao-dyn/9910008](#).
- [12] E. Gutkin, *J. Stat. Phys.* **83**, 7 (1996).
- [13] M. Wojtkowski, *Commun. Math. Phys.* **105**, 391 (1986).
- [14] S. Lepri, L. Rondoni, and G. Benettin, [chao-dyn/9909004](#).
- [15] P. Gaspard, *Adv. Chem. Phys.* **XCIX**, 369 (1997).
- [16] P. Cvitanović et al. <http://www.nbi.dk/ChaosBook>
- [17] D. Biswas, *Pramana-J. Phys.* **48**, 487 (1997).
- [18] J. F. Aarnes “An ergodic problem for R-polygons” Dept. of Mathematics, Technical University of Trondheim, Norway (unpublished,1974).
- [19] P. Gaspard and G. Nocolis, *Phys. Rev. Lett.* **65**, 1693 (1990).
- [20] P. Gaspard and J. R. Dorfman, *Phys. Rev. E* **52**, 3525 (1995).
- [21] S. Troubetzkoy, *Nonlinearity* **12**, 293 (1999).
- [22] N. Chernov, *J. Stat. Phys.* **88**, 1 (1997).